JOURNAL OF GEOPHYSICAL RESEARCH, VOL. 106, NO. C10, PAGES 22,451–22,463, OCTOBER 15, 2001

Modeling the alongshore current on barred beaches

B. G. Ruessink,[1,2] J. R. Miles,[3] F. Feddersen,[4] R. T. Guza,[5] and Steve Elgar[4]

Abstract. Mean alongshore currents observed on two barred beaches are compared with predictions based on the one-dimensional, time- and depth-averaged alongshore momentum balance between forcing (by breaking waves, wind, and 10–100 km scale alongshore surface slopes), bottom stress, and lateral mixing. The observations span 500 hours at Egmond, Netherlands, and 1000 hours at Duck, North Carolina, and include a wide range of conditions with maximum mean currents of 1.4 m/s. Including rollers in the wave forcing results in improved predictions of the observed alongshore-current structure by shifting the predicted velocity maxima shoreward and increasing the velocity in the bar trough compared with model predictions without rollers. For these data, wave forcing balances the bottom stress within the surfzone, with the other terms of secondary importance. The good agreement between observations and predictions implies that the one-dimensional assumption holds for the range of conditions examined, despite the presence of small alongshore bathymetric nonuniformities. With stronger bathymetric variations the model skill deteriorates, particularly in the bar trough, consistent with earlier modeling and laboratory studies.

1. Introduction

Models of the alongshore current in the nearshore often are based on the one-dimensional (1-D), depth-integrated, and time-averaged alongshore momentum balance between wind, wave, and tidal forcing, bottom stress, and lateral mixing [*Longuet-Higgins*, 1970; *Thornton and Guza*, 1986, among many others]. Breaking waves are the most important forcing mechanism in the surfzone, although wind [*Whitford and Thornton*, 1993; *Feddersen et al.*, 1998] and tidal [*Houwman and Hoekstra*, 1998] forcing can contribute significantly. Predictions of 1-D models, in which alongshore variations in waves and bathymetry are neglected, compare favorably with observations on (near) planar beaches [e.g., *Thornton and Guza*, 1986]. However, on barred beaches, predictions [e.g., *Church and Thornton*, 1993] of a strong, narrow current jet on the seaward side of the bar crest and near-zero flow in the bar trough differ from the observed broadly distributed (in the cross-shore) current, with maximum near or shoreward of the bar crest [*Feddersen et al.*, 1998], or even in the deepest part of the trough [*Church and Thornton*, 1993].

Model failure may result from alongshore variations in bathymetry and the neglect of rollers in the wave forcing [e.g., *Lippmann et al.*, 1995; *Reniers and Battjes*, 1997]. Alongshore bathymetric variations with length scale of O (100 m) often are observed in the nearshore [e.g., *Lippmann and Holman*, 1990] and may cause alongshore variations in wave height, wave direction, and mean water level (set-up). Model simulations [*Sancho et al.*, 1995; *Slinn et al.*, 2000] and laboratory observations [*Haller et al.*, 1997] show that these alongshore variations may alter significantly the nearshore current field, especially in the bar trough. Similarly, when the bathymetry had strong alongshore nonuniformities, the 1-D alongshore momentum balance assumption did not hold on the barred beach near Duck, North Carolina [*Feddersen et al.*, 1998]. Including rollers in the wave forcing causes a spatial lag between the dissipation of wave energy and the transfer of momentum to steady currents, thus shifting the alongshore current maximum shoreward (although not necessarily into the deepest part of the trough) and increasing the velocity in the trough [e.g., *Lippmann et al.*, 1995; *Reniers and Battjes*, 1997; *Kuriyama and Nakatsukasa*, 2000]. Comparisons with laboratory observations show that 1-D models with rollers are more accurate than models without rollers [*Reniers and Battjes*, 1997]. However, roller-based alongshore current models have not been tested over a wide range of field conditions.

Here, predictions of a 1-D alongshore current model are compared with field data from two barred beaches, Egmond aan Zee (Netherlands) and Duck, North Carolina (USA). The data span 500 (Egmond) and 1000 (Duck) hour time periods when alongshore variations in morphology were small.

[1] WL|Delft Hydraulics, Marine and Coastal Management, Delft, Netherlands

[2] Formerly at Institute for Marine and Atmospheric Research, Department of Physical Geography, Utrecht University, Utrecht, Netherlands

[3] Institute of Marine Studies, University of Plymouth, Plymouth, United Kingdom

[4] Woods Hole Oceanographic Institution, Woods Hole, Massachusetts, USA.

[5] Center for Coastal Studies, Scripps Institution of Oceanography, University of California at San Diego, La Jolla, California, USA

Paper number 2000JC000766.
0148-0227/01/2000JC000766$09.00

Model alongshore currents (section 2) are controlled by three free parameters (apparent bed roughness, wave-front slope, and eddy viscosity). Parameter values are obtained with model-data fitting at Egmond (section 3) and Duck (section 4). With a roller-based parameterization of the wave forcing, the model accurately describes the cross-shore structure of the mean alongshore current, supporting the validity of the 1-D assumption. The relative importance of the different forcing terms, bottom stress, and lateral mixing to the alongshore current and the effect of strong alongshore nonuniformities in the bathymetry are discussed in section 5. Conclusions are summarized in section 6.

2. Model Formulation

2.1. Wave Model

The wave model consists of two coupled differential equations describing the time-averaged (over many wave periods) wave and roller energy balances. With the assumption that the wave field is narrow-banded in frequency and direction, the wave energy balance is

$$\frac{d}{dx}\left(\frac{1}{8}\rho g H_{\mathrm{rms}}^2 c_g \cos\overline{\theta}\right) = -D_{br} - D_{bf}, \qquad (1)$$

where x is the cross-shore coordinate, H_{rms} is the root-mean-square wave height, ρ is water density, g is gravitational acceleration, c_g is the group velocity, $\overline{\theta}$ is the mean wave angle, and D_{br} and D_{bf} are breaking-wave dissipation and bottom friction that are modeled according to *Battjes and Janssen* [1978] and *Nielsen* [1983], respectively. Standard parameter values are used throughout ($\alpha = 1$, $\gamma = 0.5 + 0.4\tanh(33 s_0)$ [*Battjes and Stive*, 1985], where α is a dissipation parameter, γ is related to the maximum wave height, and s_0 is the deep water wave steepness). Bottom friction is not important in the surfzone where wave breaking dominates the dissipation. Linear wave theory is used to calculate c_g and Snell's law is used to determine $\overline{\theta}(x)$ from offshore measurements.

The energy balance for rollers is [*Stive and De Vriend*, 1994]

$$\frac{d}{dx}\left(2E_r c\cos\overline{\theta}\right) = -D_r + D_{br}, \qquad (2)$$

where E_r is the roller energy density (set to zero at the offshore boundary), c is the phase speed, and D_r is the roller dissipation, given by [*Duncan*, 1981; *Deigaard*, 1993]

$$D_r = \frac{2gE_r \sin\beta}{c}, \qquad (3)$$

where the wave-front slope β usually is assumed to be 0.1 or less [e.g., *Walstra et al.*, 1996]. The wave model is solved with a standard forward stepping scheme using the observed bathymetry, and offshore values of H_{rms}, wave period T, $\overline{\theta}$, and water level ζ.

2.2. Current Model

The depth- and time-averaged alongshore current velocity $\overline{v}$ is obtained from the 1-D depth-integrated and time-averaged alongshore momentum balance between wave, wind, and tidal forcing, and bottom stress and lateral mixing

$$-\frac{1}{\rho}\frac{dS_{yx}}{dx} + \frac{\tau_y^w}{\rho} - gh\frac{d\zeta}{dy} = c_f\langle|\vec{u}|v\rangle - \frac{d}{dx}\left(\nu h\frac{d\overline{v}}{dx}\right), \qquad (4)$$

where S_{yx} is the off-diagonal component of the radiation stress tensor [*Longuet-Higgins and Stewart*, 1964], τ_y^w is the alongshore wind stress, h is water depth, $d\zeta/dy$ is the tidally induced 10–100 km scale alongshore slope of the mean sea surface, c_f is a drag coefficient, $\vec{u}$ and v are the total instantaneous horizontal velocity vector and the instantaneous alongshore velocity, respectively, $\langle\ \rangle$ represents a time average over many wave periods, and ν is the depth-averaged eddy viscosity. Alongshore variations in morphology, waves, and currents are neglected, as are Earth rotation, variation of water density, and fluid acceleration (i.e., $d\overline{v}/dt$).

The wave forcing is the cross-shore gradient of S_{yx}. Using linear theory and assuming waves to be narrow-banded in frequency and direction, S_{yx} is

$$S_{yx} = \frac{1}{8}\rho g H_{\mathrm{rms}}^2 \frac{c_g}{c}\cos\overline{\theta}\sin\overline{\theta} + 2E_r\cos\overline{\theta}\sin\overline{\theta}, \qquad (5)$$

where the terms on the right-hand side are the wave and roller contribution, respectively. Using (1) with $D_{bf} \ll D_{br}$, (2) and (5) yield

$$\frac{dS_{yx}}{dx} = -\frac{\sin\overline{\theta}}{c}D_r. \qquad (6)$$

The drag coefficient c_f is parameterized with the Manning-Strickler equation [e.g., *Sleath*, 1984]

$$c_f = 0.015\left(\frac{k_a}{h}\right)^{1/3}, \qquad (7)$$

where k_a, the apparent bed roughness, is assumed to be cross-shore constant and time-independent, based on *Houwman and Van Rijn*'s [1999] coupled bedform-fluid modeling. The value of k_a is chosen to fit $\overline{v}$ observations, and the sensitivity of the results to the form of c_f is discussed in section 5.2. The velocity moment in the bottom stress formulation is parameterized as [*Feddersen et al.*, 2000]

$$\langle|\vec{u}|v\rangle = \sigma_T\overline{v}\left[1.16^2 + (\overline{v}/\sigma_T)^2\right]^{1/2}, \qquad (8)$$

where σ_T^2 is the wave-orbital velocity variance, calculated from H_{rms}, h, and T using linear wave theory. This empirical parameterization adequately represents $\langle|\vec{u}|v\rangle$ for the directionally spread random wave field at both Duck and Egmond (skill $r^2 = 0.99$ and a best fit slope of 0.97), confirming that (8) estimates measured moments more accurately than estimates based on either the weak-current ($\langle|\vec{u}|v\rangle \sim \sigma_T\overline{v}$) or strong-current ($\langle|\vec{u}|v\rangle \sim |\overline{v}|\overline{v}$) assumptions [*Feddersen et al.*, 2000].

Lateral mixing is included in (4) as a diffusion term [*Longuet-Higgins*, 1970]. Important sources of lateral mixing in the surfzone are breaking-induced turbulence [*Battjes*,

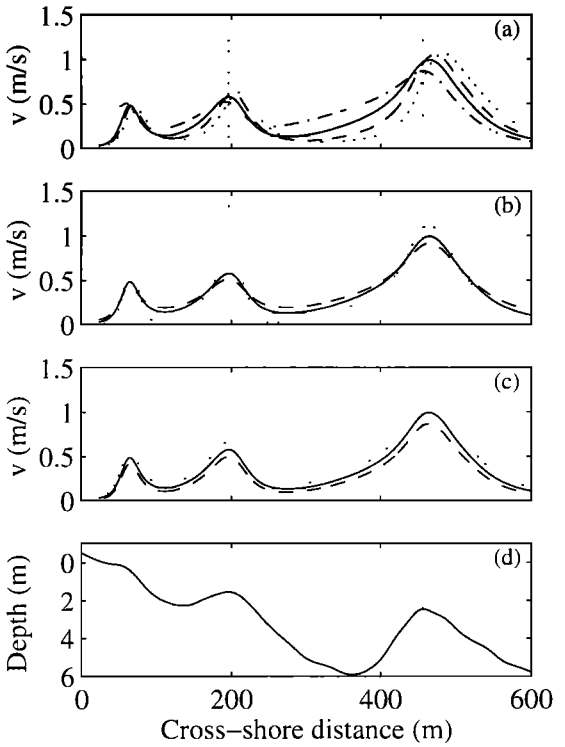

Figure 1. Alongshore current $\overline{v}$ versus cross-shore distance showing the effect of changing the wave-front slope, eddy viscosity, and apparent bed roughness. In all panels, the offshore conditions are $H_{\rm rms} = 1.5$ m, $T = 8$ s, and $\overline{\theta} = 30°$, with no wind or tidal forcing. The solid curve in Figures 1a-1c is the standard run ($\beta = 0.1$, $\nu = 0.5$ m^2/s, $k_a = 0.03$ m). Other curves correspond to changes in one parameter with the others held constant: (a) no roller (dotted line), $\beta = 0.2$ (dashed line), and $\beta = 0.05$ (dash-dotted line), (b) $\nu = 0$ m^2/s (dotted line) and $\nu = 1$ m^2/s (dashed line), and (c) $k_a = 0.015$ m (dotted line) and $k_a = 0.06$ m (dashed line). (d) The depth profile was measured at Egmond. The dotted vertical lines in each plot indicate the bar crest positions.

1975], depth variation in the cross-shore and alongshore velocities [*Svendsen and Putrevu*, 1994], and shear waves [*Özkan-Haller and Kirby*, 1999]. However, the cross-shore distribution of ν is not understood well, and for simplicity, a cross-shore constant and time-independent ν is assumed.

The modeled cross-shore distribution of D_r, c, $\overline{\theta}$, and σ_T, and the observed bathymetry, alongshore wind stress, and large-scale sea-surface slope are input into the current model, which is solved iteratively. The offshore and shoreline boundary condition for (4) are $d\overline{v}/dx = 0$, implying no diffusion of momentum through the boundaries.

2.3. Free parameters

The influence of wave-front slope β, eddy viscosity ν, and the apparent bed roughness k_a on the model $\overline{v}$ is examined using typical Egmond waves and bathymetry (Figure 1). With $k_a = 0.03$ m, (7) results in $c_f \approx 3.5 - 4.0 \times 10^{-3}$ across the inner bar and trough. With no roller, narrow current jets are located on the seaward side of each bar and near the shoreline, with near-zero currents in the troughs, qualitatively similar to the model predictions of *Church and Thornton* [1993] (Figure 1a). The roller shifts the maximum mean alongshore current $\overline{v}_{\rm max}$ onshore and broadens the current jets by increasing $\overline{v}$ in the troughs (compare dotted with solid curves in Figure 1a). The magnitude of the onshore shift in $\overline{v}_{\rm max}$ and increase in trough $\overline{v}$ is related to the advection length of the roller, which increases with decreasing β (Figure 1a) and increasing c (e.g., with increasing wave period and water depth over the bar crest). Lateral mixing smooths the cross-shore distribution of $\overline{v}$ without shifting the location of $\overline{v}_{\rm max}$ (Figure 1b). An increase in k_a decreases the magnitude of $\overline{v}$, without significantly altering the cross-shore shape of $\overline{v}$ (Figure 1c). A doubling of k_a to 0.06 m results in only a 15–20% decrease in $\overline{v}$, consistent with (7).

3. Egmond

3.1. Observations

Data were collected during October and November 1998 near Egmond aan Zee, Netherlands. The site is characterized by two well-developed bars (Figure 2). Offshore wave conditions ($H_{\rm rms}$, significant zero-downcrossing period, and $\overline{\theta}$, energy-weighted mean direction [*Kuik et al.*, 1988]) were measured by a directional wave buoy, located in 16-m depth, 5 km offshore. Winds measured 10 m above mean sea level at position P1 (Figure 2) are used to estimate wind stress. Estimates of alongshore water level gradients are obtained from observations at two tidal stations separated in the alongshore by 30 km and centered around Egmond.

Bidirectional current meters and pressure sensors were deployed on a cross-shore transect across the inner bar with an additional pressure sensor (P1) offshore of the outer bar (Figure 2). Data from P1-P6 were acquired for $\sim$ 34 min per hour (starting at each whole clock hour) at a sampling rate of 2 or 4 Hz. At P7 and P8, 10-min average velocities were stored. For comparison with $\overline{v}$ at P3-P6, the first three 10-min values of each hour are averaged. Current meter elevations above the bed were less than 1 m and varied as the morphology changed. Data are discarded when the current meters were within 0.2 m of the bed. The median grain size at the inner bar was $\sim$ 225 μm.

Spatially extensive nearshore bathymetric surveys were obtained every few days with an amphibious vehicle. The inner-bar crest, originally located 200 m from the shoreline, migrated 40 m farther offshore (Figure 3a). Bathymetric alongshore nonuniformities were always detectable (Fig-

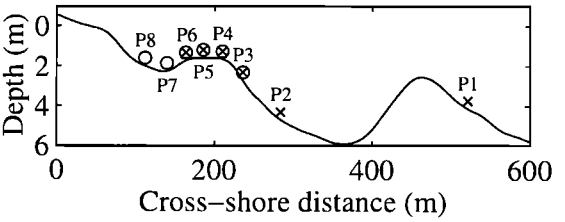

Figure 2. Depth relative to mean sea level versus cross-shore distance on October 16, 1998, at Egmond and locations of current meters (circles) and pressure sensors (crosses).

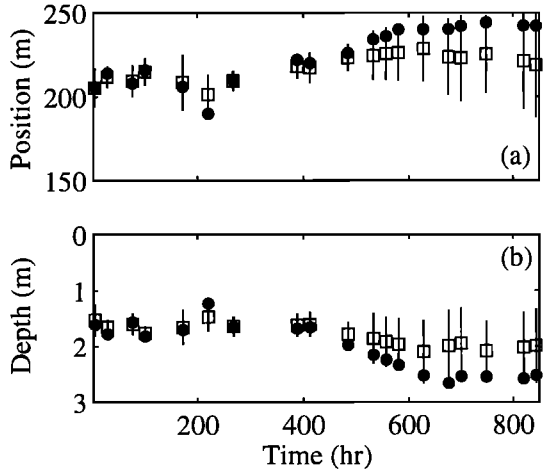

Figure 3. (a) Location of the inner bar crest location on the main measurement transect (solid circles) and location of the bar crest averaged over a 350-m wide alongshore region centered on the main transect (squares) and (b) depth above the inner bar crest at the main transect (solid circles) and averaged over a 350-m wide alongshore region (squares) versus time at Egmond. The vertical lines are ± one standard deviation. Time = 0 corresponds to October 15, 1998, 09:00 MET.

ure 3) but were most pronounced after $t \approx 500$ hours when a broad cross-shore channel developed close to the measurement transect.

A wide range of conditions were encountered. In 16-m depth, H_{rms} ranged between 0.2 and 3.9 m (Figure 4a), significant periods between 3.9 and 10.8 s, and $\overline{\theta}$ between ±45° (Figure 4b), where positive $\overline{\theta}$ indicates waves incident from the southwest. S_{yx}/ρ, computed with (5) and $E_r = 0$, ranged from -5.3 to 3.7 $\mathrm{m^3/s^2}$ (Figure 4c), and wind stress estimates τ_y^w/ρ, computed from the observed wind speed and direction with a standard formulation and a drag coefficient of 0.002, varied between -4.4 and 8.6 $\times 10^{-4}$ $\mathrm{m^2/s^2}$ (Figure 4d). The neap (spring) tidal range was ~ 1.4 (2.1) m. The alongshore surface slope varied semidiurnally owing to tides and reached maximum values of $\pm 2 \times 10^{-5}$ m/m (Figure 4e). The observed $|\overline{v}_{\mathrm{max}}|$ ranged from 0.1 to 1.3 m/s (Figure 4f). During the first 500 hours, $\overline{v}_{\mathrm{max}}$ was located near or shoreward of the bar crest (P4-P6), and afterwards $\overline{v}_{\mathrm{max}}$ was located mainly in the deepest part of the trough (P7). A tidal variation in the $\overline{v}_{\mathrm{max}}$ location [*Thornton and Kim*, 1993] was not observed.

3.2. Model-Data Comparison

The 1-D wave and current models assume alongshore uniformity in morphology, waves, and currents, so the model-data comparison is restricted to the first 500 hours of observations. Modeled and observed H_{rms} agree (Figure 5) with skill $r^2 > 0.89$ at all sensors and show the transition from H_{rms} that are closely related to offshore H_{rms} (compare P1 in Figure 5 with Figure 4a) to depth-limited and tidally modulated H_{rms} over the inner bar (e.g., P5 and P6). Root-mean-square errors ϵ_{rms} for individual sensors vary between 0.10 and 0.16 m, with an average of 0.13 m for all sensors. Wave heights at the inner bar crest (P5 and P6) are overestimated by 0.10–0.15 m, with larger errors at low tide than at high tide, and maximum differences of ~ 0.4 m near $t \approx 340$ hours (Figure 5). Examples of the observed and predicted cross-shore distribution of H_{rms} at high, mid, and low tide are given in Figures 6a-6c, respectively.

Good agreement between measured and modeled $\overline{v}$ is obtained with $\beta = 0.05$, $\nu = 0.5$ $\mathrm{m^2/s}$, and $k_a = 0.022$ m. The $\beta = 0.05$ is about the midrange of values cited by *Walstra et al.* [1996], and $\nu = 0.5$ $\mathrm{m^2/s}$ is roughly consistent with the ν parameterization used by *Özkan-Haller and Kirby* [1999] with $M = 0.5$, which for the present conditions yielded

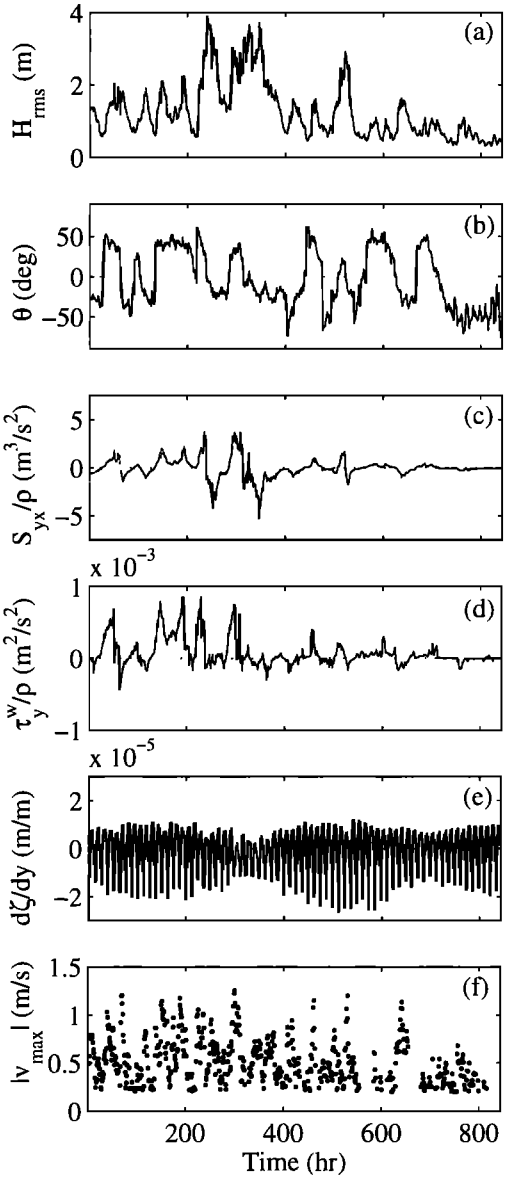

Figure 4. (a) Offshore root-mean-square wave height H_{rms}, (b) offshore wave angle $\overline{\theta}$, (c) offshore incident wave radiation stress S_{yx}/ρ, (d) alongshore wind stress τ_y^w/ρ, (e) large-scale alongshore surface slope $d\zeta/dy$, and (f) absolute maximum alongshore velocity $|\overline{v}_{\mathrm{max}}|$ versus time at Egmond. The 599 shown values in Figure 4f correspond to situations with at least four active current meters and $|\overline{v}_{\mathrm{max}}| > 0.2$ m/s.

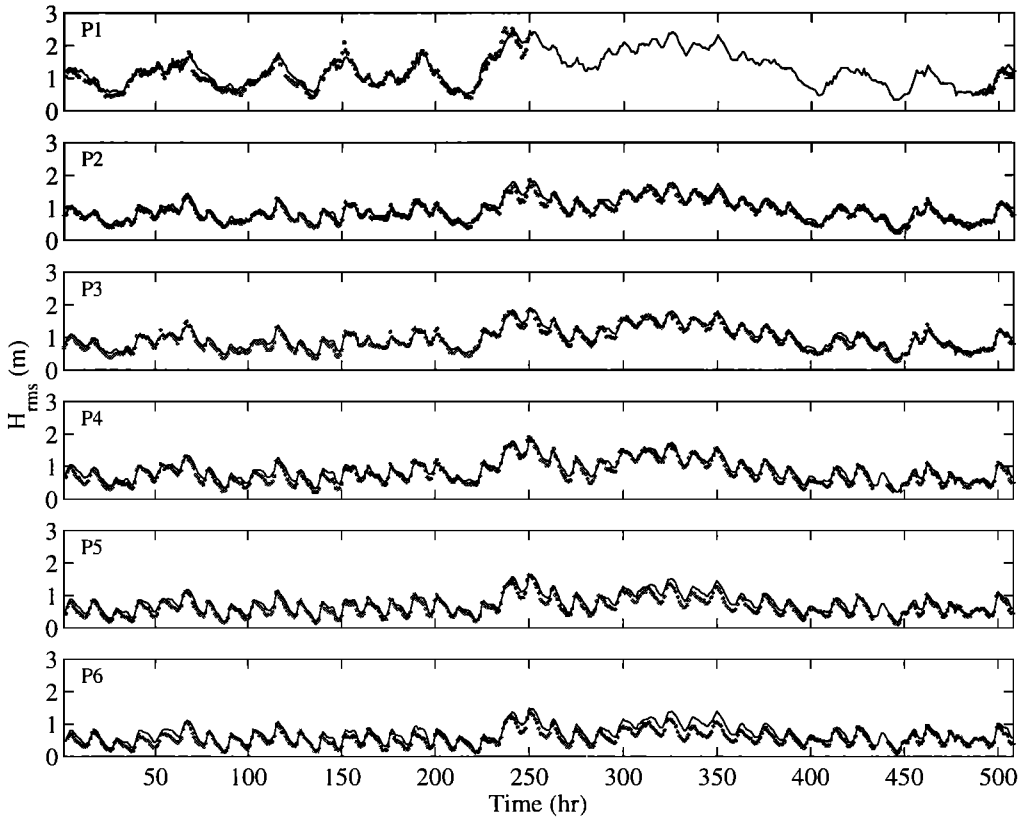

Figure 5. Measured (symbols) and modeled (lines) H_{rms} from offshore (P1) to onshore (P6) versus time at Egmond.

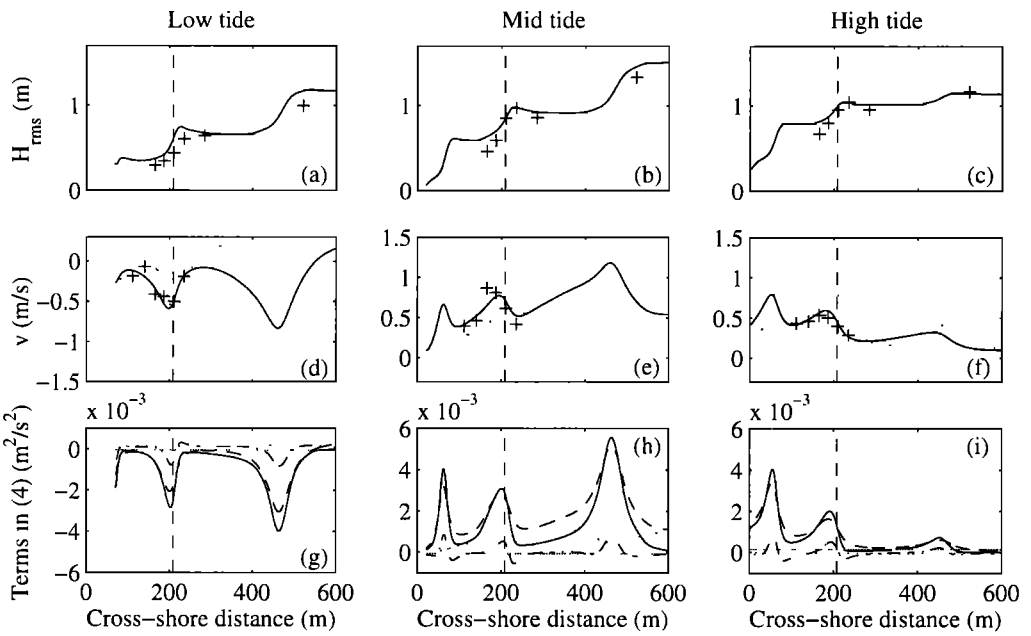

Figure 6. Measured (symbols) and modeled (lines) (a)-(c) H_{rms} and (d)-(f) $\overline{v}$ (solid line, roller; dotted line, no roller) at Egmond, and (g)-(i) terms of the alongshore momentum balance (solid line, wave forcing (roller model); horizontal gray line, wind forcing; dotted line, tidal forcing; dashed line, bottom stress; and dash-dotted line, lateral mixing) versus cross-shore distance. Columns from left to right: low tide (t = 76 hours), mid tide (t = 52 hours), and high tide (t = 56 hours). The location of the inner-bar crest, x = 208 m, is shown with a vertical dashed line.

Table 1. Alongshore Current Model Error Statistics at Egmond ($k_a = 0.022$ m, $\nu = 0.5$ m^2/s)[a]

	Roller ($\beta = 0.05$)			No Roller		
	ϵ_{rms}, m/s	m	r^2	ϵ_{rms}, m/s	m	r^2
P3	0.14	0.93	0.88	0.25	1.32	0.85
P4	0.17	1.03	0.90	0.29	1.39	0.90
P5	0.15	0.95	0.91	0.19	0.75	0.89
P6	0.17	0.86	0.92	0.29	0.53	0.90
P7	0.13	1.00	0.91	0.19	0.58	0.88
P8	0.14	0.86	0.90	0.19	0.63	0.88

[a]Here, ϵ_{rms} is the root mean square error between modeled and observed $\overline{v}$, m and r^2 are the slope and correlation coefficient of least squares fits between modeled and observed $\overline{v}$. A value of $m > 1$ corresponds to model overprediction of the observed $\overline{v}$.

a range of cross-shore averaged ν between 0.1–0.9 m^2/s. With $k_a = 0.022$ m, bar-crest c_f ranges depending on the tide from 2.6×10^{-3} to 5.2×10^{-3}, within the range of previously determined surfzone c_f [*Feddersen et al.*, 1998; *Garcez-Faria et al.*, 1998]. Average c_f are 5–15% lower in the trough than on the bar crest. With these free model parameter values, the cross-shore distribution of $\overline{v}$ is reproduced accurately (Figure 7) with skill $r^2 \geq 0.88$, best-fit slopes m between 0.86 and 1.03, and $\epsilon_{\text{rms}} < 0.2$ m/s (Table 1, roller run). The predicted $\overline{v}_{\max}$ location is between the bar crest at P4 and the shoreward side of the bar at P6 (e.g., Figures 6d-6f), with a tidally induced cross-shore variation of 10–30 m, similar to the distance between sensors, possibly explaining why a tidal variation in $\overline{v}_{\max}$ location was not observed. The relatively poor H_{rms} prediction at P5 and P6 at $t \approx 340$ hours (Figure 5) does not result in poor $\overline{v}$ prediction (Figure 7). The good agreement between modeled and measured $\overline{v}$ indicates that the use of cross-shore constant and time-independent values of β, ν, and k_a at Egmond is reasonable.

The effect of the roller is shown by running the model with the same $\nu = 0.5$ m^2/s and $k_a = 0.022$ m but without the roller (Table 1, no roller run). Neglecting the roller causes an immediate transfer of momentum from organized wave motion to $\overline{v}$, resulting in overprediction of $\overline{v}$ seaward of the bar crest (P3-P4; best-fit slope $m \approx 1.3$–1.4) and underprediction of $\overline{v}$ on the shoreward side of the bar and in the trough (P6-P8; $m \approx 0.5$–0.6). In comparison with the roller run, ϵ_{rms} are increased 25–80%. The predicted $\overline{v}_{\max}$ location is $\sim$ 10 m seaward of the bar crest, with about a 10 m tidal variation, less than predicted with rollers. The degraded model performance without rollers is most marked at mid and high tide (Figures 6d-6f), when the roller-induced onshore shift in $\overline{v}_{\max}$ location and the increase in trough $\overline{v}$ are largest.

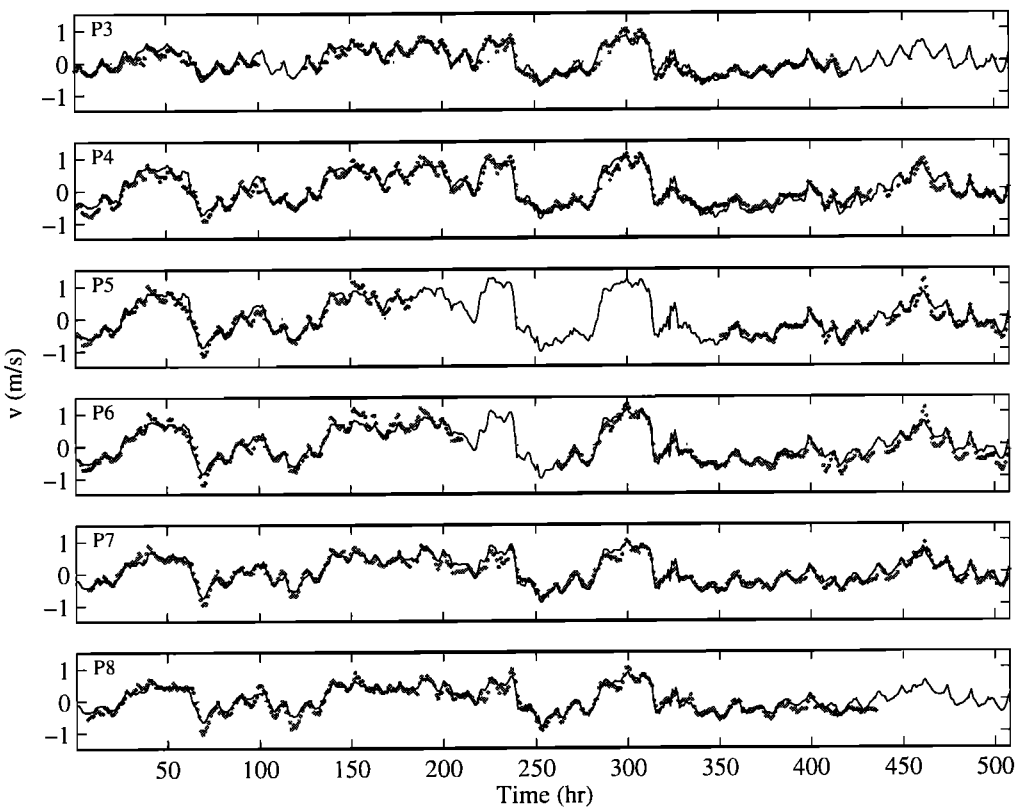

Figure 7. Measured (symbols) and modeled (lines) $\overline{v}$ from offshore (P3) to onshore (P8) versus time at Egmond. Error statistics are given in Table 1, roller run.

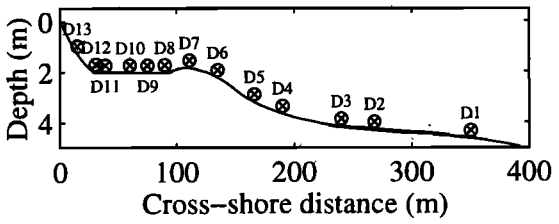

Figure 8. Depth relative to mean sea level versus cross-shore distance on September 14, 1994, at Duck and locations (symbols) of colocated current meters and pressure sensors.

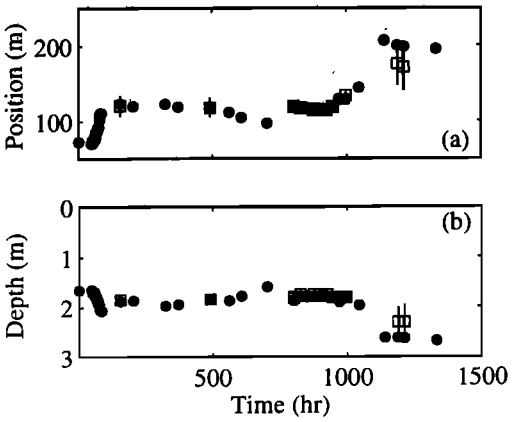

Figure 9. (a) Location of the bar crest location on the main measurement transcect (solid circles) and location of the bar crest averaged over a 350-m wide alongshore region centered on the main transect (squares) and (b) mean depth above the bar crest at the main transect (solid circles) and averaged a 350-m wide alongshore region (squares) versus time at Duck. Time = 0 corresponds to September 1, 1994, 01:00 EST. The vertical lines are ± one standard deviation.

4. Duck

4.1. Observations

The Duck data were collected from September 1 until October 31, 1994, during the Duck94 experiment at the U.S. Army Corps of Engineers Field Research Facility (FRF) near Duck, North Carolina, on a barrier island in the Atlantic Ocean. Wave statistics (H_{rms}, peak period, and energy-weighted $\overline{\theta}$ [*Kuik et al.*, 1988]) in 8-m water depth were estimated from a two-dimensional (2-D) array of 15 bottom-mounted pressure sensors [*Long*, 1996]. Wind stress estimates are obtained from winds measured 19.5 m above mean sea level at the end of the nearby FRF pier. Alongshore surface slopes are computed from two pressure sensors separated by 30 km (centered around Duck) along the 5-m isobath [*Lentz et al.*, 1999]. Pressure and velocity observations were obtained at 13 cross-shore positions (Figure 8) extending from near the shoreline to 4.5-m depth. Details on data acquisition and processing are given by *Elgar et al.* [1997], *Gallagher et al.* [1998], and *Feddersen et al.* [1998]. The mean grain size along the transect varied between 180–250 μm [*Gallagher et al.*, 1998].

Spatially extensive bathymetric surveys obtained occasionally with an amphibious vehicle and cross-shore depth profiles obtained continuously with altimeters [*Gallagher et al.*, 1998] show that the bar migrated offshore 120 m during the experiment but only 50 m during the first 1000 hours

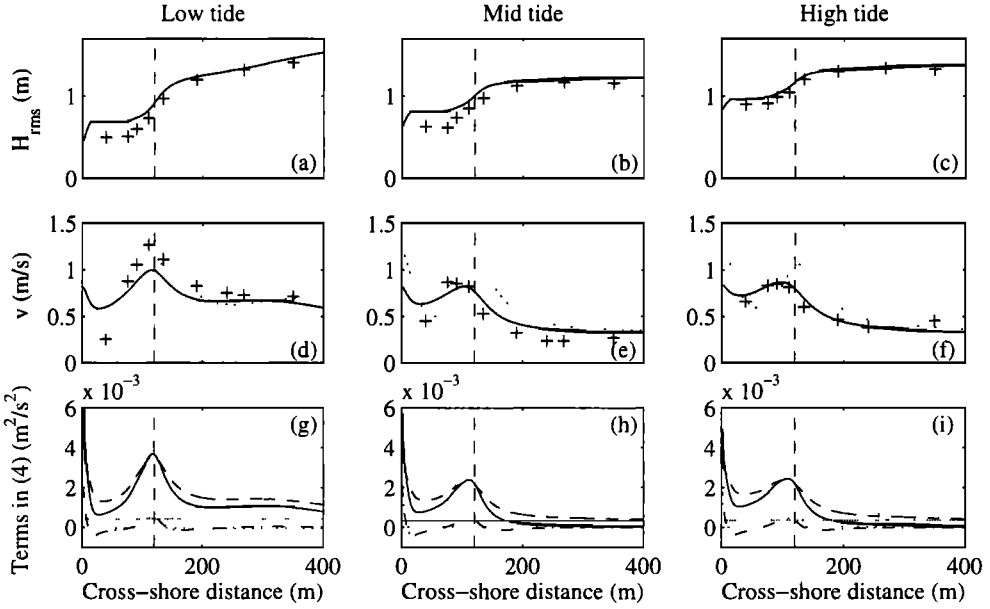

Figure 10. Measured (symbols) and modeled (lines) (a)-(c) H_{rms} and (d)-(f) $\overline{v}$ (solid line, roller; dotted line, no roller) at Duck, and (g)-(i) terms of the alongshore momentum balance (solid line, wave forcing (roller model); horizontal gray line, wind forcing; dotted line, tidal forcing; dashed line, bottom stress; and dash-dotted line, lateral mixing) versus cross-shore distance. Columns from left to right: low tide (t = 780 hours), mid tide (t = 776 hours), and high tide (t = 785 hours). The location of the inner-bar crest, x = 120 m, is shown with a vertical dashed line.

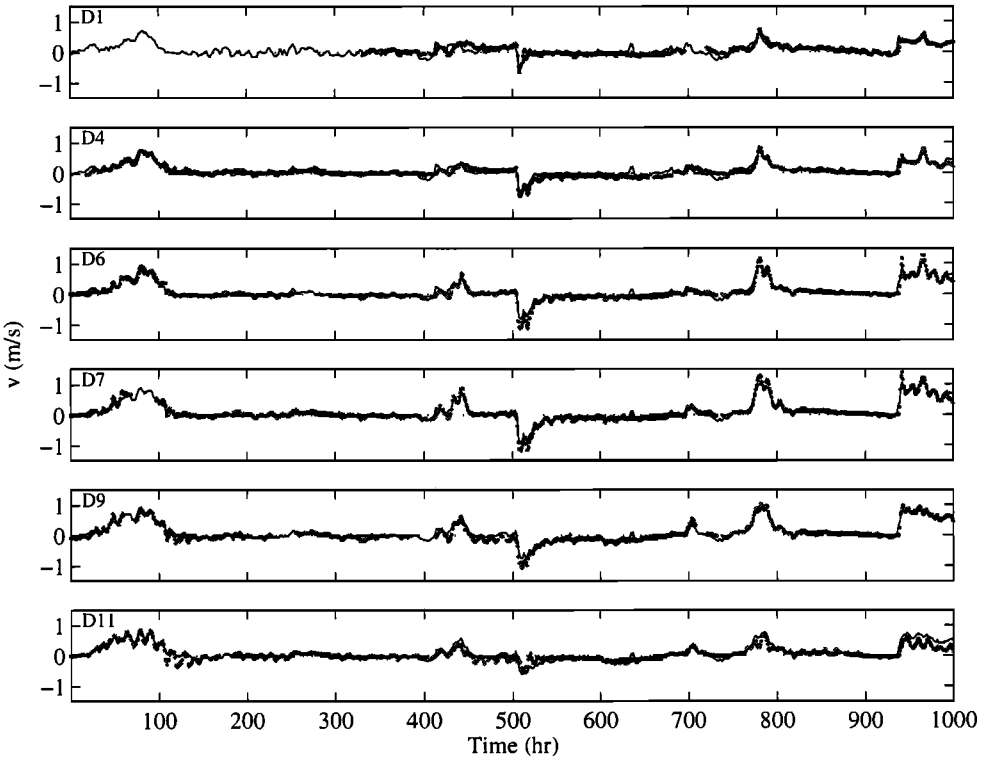

Figure 11. Measured (symbols) and modeled (lines) alongshore mean current $\overline{v}$ versus time at Duck from offshore (D1) to onshore (D11). Error statistics are given in Table 2, roller run.

(Figure 9a). Alongshore nonuniformities in the bar were small for $t < 1000$ hours (Figure 9), when a broad cross-shore channel developed near the measurement transect.

In 8-m depth, 750 m from shore, $H_{\rm rms}$ ranged between 0.1 and 2.9 m, peak periods between 3 and 16 s, and $\overline{\theta}$ between $\pm$ 50°. Estimates of S_{yx}/ρ, computed with (5) and $E_r = 0$, ranged between -1.0 and 0.9 m^3/s^2, less than 25% of the maximum values at Egmond. Wind stress estimates, τ_y^w/ρ, varied between -2.5 and 7.1×10^{-4} m^2/s^2. The tide was semidiurnal with a spring range of 1 m. Compared with Egmond, the alongshore surface slopes were small, generally less than 3×10^{-6} m/m. Alongshore current maxima reached absolute values up to 1.4 m/s, and the largest $|\overline{v}_{\rm max}|$ (greater than $\sim$ 0.5 m/s) were located near the bar crest [*Feddersen et al.*, 1998]. The $|\overline{v}_{\rm max}|$ location was tidally modulated, shifting from near the bar crest at low tide to 30 m farther shoreward at high tide.

4.2. Model-Data Comparison

Model-data comparison is restricted to the first 1000 hours, when alongshore bathymetric nonuniformities were small (Figure 9). Excluding calm conditions (offshore $H_{\rm rms} \leq 0.5$ m), the wave height prediction error $\epsilon_{\rm rms}$ varies between 0.04 and 0.11 m, with an average of 0.08 m for all sensors, slightly less than at Egmond. Skill r^2 exceeds 0.8 from D1 to D10, demonstrating that the observed tidally modulated wave field at the bar crest and in the trough (not shown, but similar to Egmond, Figure 5) is reproduced accurately. Similar to Egmond, the differences in the trough are smallest at high tide (0–0.1 m) and increase to 0.1–0.2 m at low tide (Figures 10a-10c).

With the Egmond $\overline{v}$ model parameters ($\beta = 0.05$, $\nu = 0.5$ m^2/s, and $k_a = 0.022$ m), modeled and measured $\overline{v}$ (not shown) are correlated ($r^2 \geq 0.75$), but the predictions are smaller than the observations (best-fit $m < 1$). Reducing k_a to 0.0125 m (a 20% c_f reduction compared with Egmond) results in improved model predictions (Figure 11 and Table 2, roller run). The reasons for the k_a differences are unknown and the parameterization and variation of c_f are not understood (see section 5.2). With $k_a = 0.0125$ m, c_f on the bar crest ranges depending on the tide from 2.4×10^{-3} to 3.3×10^{-3}, with an average of 2.7×10^{-3}. Trough c_f are $3 - 10\%$ lower. These c_f are similar to previous surfzone-averaged estimates of $c_f = 3.3 \times 10^{-3}$ [*Feddersen et al.*, 1998]. The best-fit slopes m range from 0.86 to 1.07 (D5-D12), and $\epsilon_{\rm rms}$ is 0.1 m/s, increasing to 0.2 m/s close to the shore (Table 2). The approximately constant best-fit slopes (with values near one) across the bar into the trough indicate that the cross-shore structure of the alongshore mean current is reproduced reasonably well, except near the shoreline (D13) where the observed $\overline{v}$ is overpredicted by $\sim$ 25%. Consistent with observations, the predicted $\overline{v}_{\rm max}$ location is near the bar crest at low tide, shifting 15–25 m shoreward at high tide.

The $\overline{v}$ model performance is tidally modulated (Figures 10d-10f). At high and mid tide, the predicted cross-shore structure of $\overline{v}$ agrees well with the observations (Figures 10e-10f). At low tide (Figure 10d) the $\overline{v}_{\rm max}$ location is repro-

Table 2. Alongshore Current Model Error Statistics at Duck ($k_a = 0.0125$ m, $\nu = 0.5$ m^2/s)[a]

	Roller ($\beta = 0.05$)			No Roller		
	ϵ_{rms}, m/s	m	r^2	ϵ_{rms}, m/s	m	r^2
D1	0.11	0.82	0.76	0.11	0.94	0.77
D2	0.10	0.85	0.83	0.11	0.91	0.84
D3	0.09	0.87	0.88	0.09	0.92	0.88
D4	0.10	0.86	0.88	0.12	1.02	0.88
D5	0.12	0.96	0.87	0.11	1.01	0.85
D6	0.10	0.86	0.96	0.18	1.14	0.92
D7	0.10	0.88	0.96	0.14	0.87	0.92
D8	0.09	0.90	0.97	0.19	0.70	0.89
D9	0.10	0.88	0.96	0.20	0.61	0.89
D10	0.11	1.01	0.91	0.12	0.75	0.92
D11	0.17	1.03	0.80	0.15	0.91	0.80
D12	0.21	1.07	0.77	0.19	1.08	0.79
D13	0.23	1.27	0.75	0.33	1.74	0.81

[a] To exclude the frequent periods of near zero flow (e.g., Figure 11), the statistics were based on observations only with $|\overline{v}_{\max}| > 0.2$ m/s and at least five active current meters between (and including) D5 to D12. The number of these observations ranged from 133 at D5 to 352 at D8.

duced accurately, but the overall modeled $\overline{v}$ distribution is broader than observed. Similar discrepancies occur during other tidal cycles with strong currents. The different breaker types (e.g., plunging or spilling) that may occur at different tide levels are not accounted for and may contribute to model errors. With $k_a = 0.0125$ m and $\nu = 0.5$ m^2/s, but without the roller, the model (Table 2, no roller run) overpredicts $\overline{v}$ on the seaward side of the bar (D6, $m \approx 1.1$) and strongly underpredicts $\overline{v}$ in the trough (D8-D11, $m \approx 0.6$–0.9). Similar to Egmond, the model improvement from including the roller into the wave-forcing parameterization is greatest at mid and high tide, when roller advection distances are largest (Figures 10e-10f).

5. Discussion

5.1. Importance of Dynamical Terms

Although Egmond and Duck differ in incident wave conditions and morphology (i.e., double and single bar systems), the alongshore momentum balances are similar. For example, in the three cases at different tidal stages, the wave forcing largely balances the surfzone bottom stress, and wind forcing, tidal forcing, and lateral mixing are secondary terms but cannot in general be neglected (Figures 6g-6i and 10g-10i). Lateral mixing is most important near the current jets, where it reduces $|\overline{v}_{\max}|$ and broadens $\overline{v}(x)$. Seaward of the surfzone, the bottom stress balances the wind and tidal forcing at Egmond and roughly balances wind forcing at Duck (Figures 6g-6i and 10g-10i). The low-tide wave forcing typically is stronger, narrower, and farther offshore than the high-tide wave forcing (e.g., Figures 10g-10i), resulting in different alongshore current distributions (Figure 10d-10f).

Estimates of the importance of the model terms (4) are obtained by spatially averaging the absolute value of each term across the bar-trough region (Egmond: $110 \le x \le 235$ m, P3-P8; Duck: $30 \le x \le 165$ m, D5-D12) for each run, and calculating the rms value for the entire experiment (Table 3). The rms wave and wind forcing at Duck are each half those at Egmond, reflecting the less energetic conditions at Duck. At both sites the waves are the dominant forcing mechanism and largely balance the bottom stress (Table 3, roller run). Wind forcing is 20–25% of the wave forcing over the bar-trough region at both sites. Tidal forcing is, on average, as significant as wind forcing at Egmond but is negligible at Duck [*Feddersen et al.*, 1998; *Lentz et al.*, 1999]. Tidal forcing at Egmond results in semidiurnal currents with amplitude 0.3–0.5 m/s when wind forcing is weak. At both sites, rollers alter the spatial structure of the wave forcing but not the rms wave forcing integrated over the bar-trough region (Table 3, compare roller with no roller runs). However, without rollers, the rms lateral mixing approximately doubles owing to the narrower spatial distribution of wave forcing and $\overline{v}$.

The wave forcing with and without rollers also was averaged separately over the bar crest (Egmond: $165 \le x \le 235$ m, P3-P6; Duck: $90 \le x \le 165$ m, D5-D8) and trough (Egmond: $110 \le x < 165$ m, P3-P6; Duck: $30 \le x < 90$ m, D8-D12) regions (not shown). At both sites, the rms wave forcing without rollers is largely concentrated at the bar crest, and the trough rms wind and wave forcing are approximately equal. The roller changes the wave-forcing distribution, causing the bar and trough rms wave forcing to be approximately equal, resulting in improved model-data $\overline{v}$ agreement.

5.2. The c_f Parameterizations

The ratio of roughness to depth k_a/h is believed to influence c_f and is utilized in the Manning-Strickler c_f parameterization (7) implemented here. The cross-shore and temporally constant k_a is suggested by coupled bedform-fluid modeling [*Houwman and Van Rijn*, 1999] but is inconsistent with k_a estimates based on vertical profile measurements of

Table 3. Root-Mean-Square Values ($\times 10^{-3}$ m^2/s^2) of Terms in the Alongshore Momentum Balance Integrated Over the Bar-Trough Region

	Egmond		Duck	
	Roller	No Roller	Roller	No Roller
Wave forcing	1.28	1.27	0.61	0.58
Wind forcing	0.25	0.25	0.14	0.14
Tidal forcing	0.20	0.20	0.02	0.02
Bottom stress	1.41	1.34	0.71	0.71
Lateral mixing	0.19	0.44	0.08	0.18

Table 4. Selected Alongshore Current Model Error Statistics With Different c_f Parameterizations ($\beta = 0.05$, $\nu = 0.5\ m^2/s$)

	$c_f \sim k_a/h$ (7)			c_f = Constant		
	ϵ_{rms}, m/s	m	r^2	ϵ_{rms}, m/s	m	r^2
			Egmond[a]			
P3	0.14	0.93	0.88	0.18	0.63	0.84
P5	0.15	0.95	0.91	0.19	1.07	0.89
P8	0.14	0.86	0.90	0.18	0.72	0.88
			Duck[b]			
D1	0.11	0.82	0.76	0.12	0.65	0.75
D7	0.10	0.88	0.96	0.10	0.86	0.97
D11	0.17	1.03	0.80	0.18	1.02	0.79

[a] $k_a = 0.022$ m and $c_f = 3.2 \times 10^{-3}$.
[b] $k_a = 0.0125$ m and $c_f = 2.7 \times 10^{-3}$.

the alongshore current at Duck, where k_a was found to vary from 0.01–2.1 m ($k_a = 30z_a$, *Garcez-Faria et al.* [1998, Table 1]). Therefore, although (7) with cross-shore constant and time-independent k_a yields accurate $\overline{v}$ predictions, k_a may not be modeled accurately.

For simplicity, the drag coefficient c_f commonly is assumed to be cross-shore constant [e.g., *Thornton and Guza*, 1986; *Reniers and Battjes*, 1997] and not to depend on k_a/h as used here (7). At Egmond, cross-shore constant $c_f = 3.2 \times 10^{-3}$ (the bar-trough average from (7)) leads to a moderate increase in ϵ_{rms} of several cm/s (Table 4). The bar crest (P5) $\overline{v}$ is overpredicted slightly, and the offshore (P3) and trough (P8) $\overline{v}$ are underpredicted significantly (Table 4). With the bar-trough average $c_f = 2.7 \times 10^{-3}$, the offshore (D1) $\overline{v}$ at Duck also is underpredicted, but the bar (D7) and trough (D11) $\overline{v}$ model-data error and regression slope m are similar to those with (7) (Table 4). The constant c_f Duck $\overline{v}$ predictions in the trough may not be as degraded as at Egmond because the bar-trough depth difference at Duck is smaller than at Egmond (compare Figure 2 with Figure 8), which according to (7) leads to a smaller difference between bar and trough values of c_f. The offshore $\overline{v}$ underprediction with constant c_f at both Egmond and Duck indicates that the offshore c_f should be reduced relative to the bar-trough average, consistent with integrated momentum balances [*Feddersen et al.*, 1998]. This suggests that, in general, a cross-shore varying c_f, reduced in the trough and offshore and increased at the bar crest, such as parameterized by (7), yields improved $\overline{v}$ predictions.

Although (7) yields accurate $\overline{v}$ predictions when k_a is chosen to match observations, the appropriate a priori value of k_a is not known. The average offshore S_{yx} is overestimated owing to the assumption of a narrow-band in $f - \theta$ wave field (appendix A). This causes a positive bias in the model wave forcing and thus an overestimation of k_a and hence c_f. At Duck, S_{yx} is overestimated on average by $\sim$ 60% (appendix A) and thus c_f using a more accurate S_{yx} would be roughly 60% of the values used here. The S_{yx} overestimation will differ from site to site and may contribute to the difference in k_a at Egmond and Duck.

The k_a used here with (7) should not be interpreted as an apparent roughness height. The Duck k_a is slightly less than the rms physical roughness, but the expected amplification from wave-current interaction is $O(10 - 100)$ [*Houwman and Van Rijn*, 1999]. Wave breaking may also increase c_f [e.g., *Church and Thornton*, 1993] and thus contribute to the increased bar-trough c_f relative to offshore, where wave breaking was infrequent. The form of (7), $c_f \sim h^{-1/3}$, indirectly may incorporate breaking-wave effects. Given the bias in the wave forcing, the problematic assumptions of (7), and the possible inconsistency between modeled k_a and the physical roughness and expected amplification factor, the k_a in (7) is best interpreted as a free model parameter that when chosen appropriately yields accurate $\overline{v}$ predictions and c_f values within the range of previously determined c_f.

5.3. Two-Dimensional Conditions

The high skill and best-fit slopes near one between measured and modeled currents implies that the assumption of 1-D morphology, waves, and currents is valid for the range of conditions examined ($t < 500$ hours at Egmond, $t < 1000$ hours at Duck). Apparently, 2-D terms (such as local alongshore pressure gradients) are small relative to the 1-D terms. Larger morphological nonuniformities that developed later did not affect H_{rms} predictions ($\epsilon_{rms} = 0.08$ and 0.09 m for all sensors at Egmond and Duck, respectively). In contrast, $\overline{v}$ model skill is lower at Egmond after a rip channel developed near the sensors. Model-data agreement seaward of the rip channel (P4) is good (Figure 12, Table 5), indicating that the 2-D terms are negligible in this region. The predictive skill of the model is lower closer to shore, where ϵ_{rms} almost doubles and the best-fit m reduces to 0.5 (Figure 12, Table 5). Furthermore, the model performance is strongly tidally modulated. At high tide, modeled and measured $\overline{v}$ agree well, but at low tide the model un-

Table 5. Selected Alongshore Current Model Error Statistics for 1-D and 2-D Periods ($\beta = 0.05$, $\nu = 0.5\ m^2/s$)

	1-D[a]			2-D[b]		
	ϵ_{rms}, m/s	m	r^2	ϵ_{rms}, m/s	m	r^2
			Egmond ($k_a = 0.022$ m)			
P4	0.17	1.03	0.90	0.10	1.10	0.79
P7	0.13	1.00	0.91	0.21	0.48	0.65
			Duck ($k_a = 0.0125$ m)			
D3	0.09	0.87	0.88	0.14	0.89	0.51
D10	0.11	1.01	0.80	0.26	0.49	0.43

[a] Egmond: $t < 500$ hrs; Duck: $t < 1000$ hrs.
[b] Egmond: $550 < t < 850$ hrs; Duck: $1000 < t < 1250$ hrs.

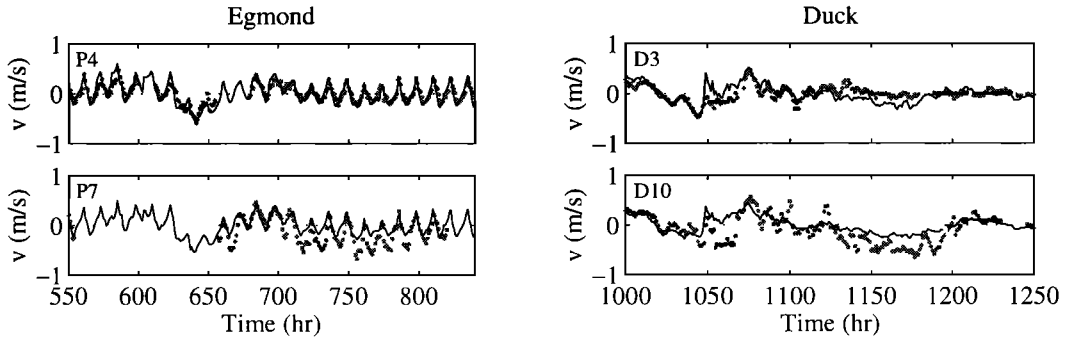

Figure 12. Measured (symbols) and modeled (lines) $\overline{v}$ with 2-D conditions versus time at (left) Egmond and (right) Duck.

derpredicts $\overline{v}$ by a factor of 3. Video time exposure images and visual observations revealed no wave breaking at high tide (i.e., the flows were tidal) and some breaking at low tide but not in the rip channel. Also, the mean cross-shore currents at P4-P7 are tidally modulated with near-zero flow at high tide and offshore directed flows of 0.6 m/s at low tide, suggesting a rip current active on a semidiurnal scale. Similar to Egmond, model skill at Duck also degrades under 2-D conditions ($1000 < t < 1250$ hours), particularly in the bar trough (D10, Figure 12, Table 5).

To examine further the effect of 2-D bathymetry on $\overline{v}$ model performance at Egmond, error statistics were computed for each period between two profile measurements and compared with a nondimensional metric of bathymetric nonuniformity, quantified for each survey as the spatially averaged and normalized squared difference between the depth $d(x, y)$ and the alongshore (y) averaged cross-shore depth profile $\overline{d}(x)$

$$\chi^2 = \frac{1}{L_x L_y} \int_0^{L_x} \int_0^{L_y} \left(\frac{d(x,y) - \overline{d}(x)}{\overline{d}(x)} \right)^2 dy\, dx. \quad (9)$$

where L_x and L_y are the cross-shore and alongshore length of the survey region, respectively. Averaged over $110 \leq x \leq 235$ m and $-175 \leq y \leq 175$ m ($y = 0$ is the main transect), χ^2 varies between 0.004–0.021 during the 1-D period ($t < 500$ hours) and increases to 0.033 afterward. Seaward of the bar (P4), the best-fit m is independent of χ^2 and scatters around 1 (open circles in Figure 13). Comparable model performance is found in the trough for $\chi^2 <\approx 0.02$, but m dropped to ≈ 0.5 for larger χ^2 (open triangles in Figure 13). During the Duck experiment, χ^2 ($30 \leq x \leq 190$ m, $-175 \leq y \leq 175$ m) was far less variable with 0.0038 ± 0.0008 (mean $\pm$ standard deviation) during the 1-D period ($t < 1000$ hours) and $\chi = 0.024 \pm 0.001$ afterward. The bar and trough best-fit m for the 1-D and 2-D period (i.e., Table 5) are comparable to those at Egmond for the same χ^2 (Figure 13). On the basis of the $\chi^2 = 0.02$ criterion, the 1-D assumption was valid for ~ 60 and 70% of time during the Egmond and Duck experiments, respectively. Note that $\chi^2 = 0.02$ corresponds to an alongshore depth variability of 14% of the mean depth. Further work is needed to determine if χ^2 is a robust indicator of 2-D effects.

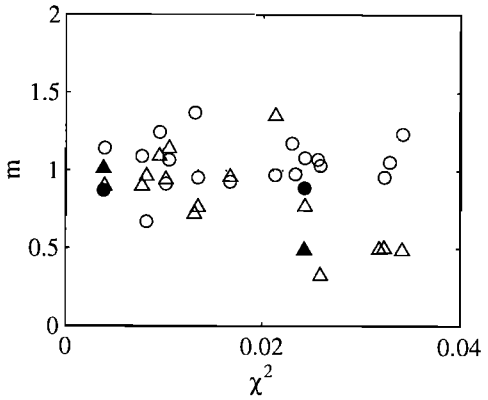

Figure 13. Best-fit slope m seaward of bar crest (circles) and in the bar trough (triangles) versus χ^2. Open symbols, Egmond P4 and P7; filled symbols, Duck D3 and D10. The two χ^2 values at Duck are averaged over the 1-D and 2-D period.

6. Conclusions

Using standard literature values [*Battjes and Stive*, 1985], the cross-shore wave height distribution is reproduced accurately, with an average root mean square error of 0.13 and 0.08 m at Egmond and Duck, respectively. The error in wave height is tidally modulated with increased error at low tide. For a wide range of conditions at both locations, the cross-shore structure of the mean alongshore current is predicted well with a 1-D alongshore current model (i.e., 2-D effects are ignored). Essential to the accurate prediction is the inclusion of rollers in the wave forcing, confirming earlier laboratory results. Rollers shift the velocity maxima shoreward and increase the alongshore flow in the trough, resulting in predictions of the mean alongshore current consistent with field observations. Within the surfzone, the model primarily balances wave forcing with bottom stress. Wind forcing, lateral mixing, and at Egmond tidal forcing, are secondary, but not negligible.

The agreement between measured and modeled mean alongshore current implies that the assumption of a time and cross-shore independent apparent bed roughness (chosen to fit the observations), wave front slope, and eddy viscosity is reasonable, and that weak nonuniformities in morphology are unimportant to the alongshore current, consistent with

previous integrated 1-D alongshore momentum balances at Duck. The Egmond roller slope and eddy viscosity work well at Duck, but for unknown reasons, bed roughness at Duck decreases almost 50% (a 20% reduction in drag coefficient). The appropriate roughness without fitting to observations is unclear. With appropriate roughness a cross-shore varying drag coefficient yields improved predictions compared with a constant drag coefficient. Additional data-model comparisons suggest that the 1-D balance does not hold, especially in the bar trough, when the bathymetry is strongly alongshore inhomogeneous, consistent with earlier model and laboratory studies.

Appendix A: Radiation Stress Estimates

The radiation stress component S_{yx} in a directionally spread random wave field seaward of the surfzone is, according to linear theory [*Battjes*, 1972],

$$S_{yx} = \int_0^\infty \int_{-\pi}^{\pi} E(f,\theta)\frac{c_g(f)}{c(f)} \sin\theta\cos\theta \, d\theta \, df, \qquad \text{(A1)}$$

where $E(f,\theta)$ is the frequency-directional (f-θ) energy spectrum, and $c_g(f)$ and $c(f)$ are the frequency dependent group and phase velocities, respectively. For a monochromatic (single frequency) and unidirectional (single wave-angle) plane wave of height H, (A1) reduces to

$$S_{yx} = \frac{1}{8}\rho g H^2 \frac{c_g}{c} \sin\theta\cos\theta, \qquad \text{(A2)}$$

where c_g and c are evaluated at the monochromatic wave frequency.

For simplicity, alongshore current models that incorporate random waves often approximate S_{yx} similar to (A2),

$$S_{yx} = \frac{1}{8}\rho g H_{\text{rms}}^2 \frac{c_g(\overline{f})}{c(\overline{f})} \sin\overline{\theta}\cos\overline{\theta}, \qquad \text{(A3)}$$

where c_g and c are evaluated at the peak or mean (energy-weighted) wave frequency $\overline{f}$ and $\overline{\theta}$ is a peak or mean (energy-weighted) wave angle. This S_{yx} approximation (A3) is accurate only for a wave field that is narrow banded in frequency and direction.

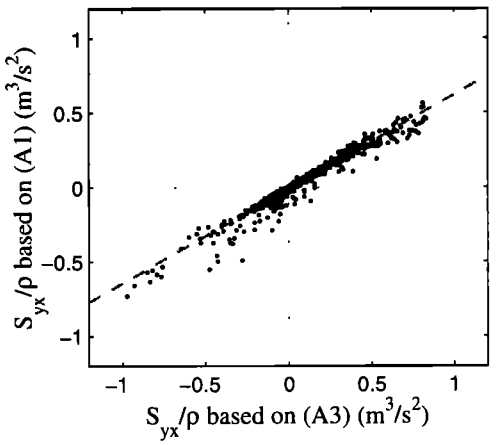

Figure A1. Offshore S_{yx}/ρ based on equation (A1) versus S_{yx}/ρ based on equation (A3) at Duck. The dashed line is the best-fit line with slope 0.63. The correlation $r = 0.98$ (1332 data points).

Accurate S_{yx} estimates based on (A1) were obtained by applying a moment-estimation method [*Elgar et al.*, 1994] to data from the FRF 8-m depth pressure sensor array [*Long*, 1996]. Corresponding S_{yx} estimates based on (A3) were made using array estimates of H_{rms}, mean (energy-weighted) $\overline{f}$, and mean (energy-weighted) $\overline{\theta}$ [*Kuik et al.*, 1988]. These two estimates are correlated (Figure A1), but estimates based on (A3) overpredict S_{yx} based on (A1) by $\sim$ 60%. Egmond S_{yx} estimates based on (A1) were not available, so for consistency, (A3) with $\overline{\theta}$ was used for both Egmond and Duck.

The tendency for (A3) to overpredict S_{yx} can be understood by considering a single-frequency but directionally spread wave field with a top-hat (with width Δ) θ distribution,

$$S(\theta) = \begin{cases} \frac{1}{2\Delta}, & \overline{\theta}-\Delta \le \theta \le \overline{\theta}+\Delta \\ 0, & \text{otherwise} \end{cases}. \qquad \text{(A4)}$$

The ratio of (A1) to (A3) is

$$\frac{\frac{1}{2\Delta}\int_{\overline{\theta}-\Delta}^{\overline{\theta}+\Delta} \sin\theta\cos\theta \, d\theta}{\sin\overline{\theta}\cos\overline{\theta}} = \frac{\sin\Delta\cos\Delta}{\Delta}, \qquad \text{(A5)}$$

which is ≤ 1 for all Δ. For narrow directional spreads ($\Delta \to 0$), the ratio (A5) approaches one. The directional width Δ can be related to the directional spread σ_θ [*Herbers et al.*, 1999], and for the Duck 8-m depth $\sigma_\theta = 30° \pm 5°$, $\Delta \approx 55°$, and the ratio (A5) ≈ 0.5, roughly consistent with the best-fit slope of 0.63. For any $S(\theta)$ symmetric about $\overline{\theta}$, the ratio of (A1) to (A3) is ≤ 1. The overprediction of S_{yx} by (A3) biases the optimal alongshore current model parameters (i.e., increases k_a, and hence c_f).

Acknowledgments. This work was part of the Coast3D project funded by the European Commission's research program MAST under contract MAS3-CT97-0086. Logistical support and background data for the Egmond site were provided by the Netherlands Rijkswaterstaat as part of the KUST*2000 research program. Pressure sensors at P1 and P2 (Egmond) were maintained and deployed by Rijkswaterstaat, and current sensors at P7 and P8 were maintained and deployed by staff from the Université de Caen. The array of current meters, sonar altimeters, and pressure sensors at Duck94 was deployed and maintained by staff from the Center for Coastal Studies. Britt Raubenheimer, Edith Gallagher, and Thomas Herbers helped collect and process the data. The 8-m array wave data and logistical support was provided by the U. S. Army Corps of Engineers Field Research Facility. We thank Steve Lentz for providing the alongshore surface slope and wind data for Duck. The Duck94 experiment was funded by the Office of Naval Research and the National Science Foundation, and the analysis was also supported by the National Ocean Partnership Program. Woods Hole Oceanographic Institution contribution 10,355.

References

Battjes, J. A., Radiation stresses in short-crested waves, *J. Mar. Res.*, *30*, 56–64, 1972.

Battjes, J. A., Modelling of turbulence in the surfzone, in *Proceed-*

ings Symposium Modeling Techniques, pp. 1050–1061, Am. Soc. of Civ. Eng., New York, 1975.

Battjes, J. A., and J. P. F. M. Janssen, Energy loss and set-up due to breaking of random waves, in *Proceedings 16th International Coastal Engineering Conference*, pp. 570–587, Am. Soc. of Civ. Eng., New York, 1978.

Battjes, J. A., and M. J. F. Stive, Calibration and verification of a dissipation model for random breaking waves, *J. Geophys. Res.*, *90*, 9159–9167, 1985.

Church, J. C., and E. B. Thornton, Effects of breaking wave induced turbulence within a longshore current model, *Coastal Eng.*, *20*, 1–28, 1993.

Deigaard, R., A note on the three dimensional shear stress distribution in a surfzone, *Coastal Eng.*, *20*, 157–171, 1993.

Duncan, J. H., An empirical investigation of breaking waves produced by a towed hydrofoil, *Proc. R. Soc. London, Ser. A*, *377*, 331–348, 1981.

Elgar, S., T. H C. Herbers, and R. T. Guza, Reflection of ocean surface gravity waves from a natural beach, *J. Phys. Oceanogr.*, *24*, 1503–1511, 1994.

Elgar, S., R. T. Guza, B. Raubenheimer, T. H. C. Herbers, and E. L. Gallagher, Spectral evolution of shoaling and breaking waves on a barred beach, *J. Geophys. Res.*, *102*, 15,797–15,805, 1997.

Feddersen, F., R. T. Guza, S. Elgar, and T. H. C. Herbers, Alongshore momentum balances in the nearshore, *J. Geophys. Res.*, *103*, 15,667–15,676, 1998.

Feddersen, F., R. T. Guza, S. Elgar, and T. H. C. Herbers, Velocity moments in alongshore bottom stress parameterizations, *J. Geophys. Res.*, *105*, 8673–8686, 2000.

Gallagher, E. L., S. Elgar, and R. T. Guza, Observations of sand bar evolution on a natural beach, *J. Geophys. Res.*, *103*, 3203–3215, 1998.

Garcez-Faria, A. F., E. B. Thornton, T. P. Stanton, C. V. Soares, and T. C. Lippmann, Vertical profiles of longshore currents and related bed shear stress and bottom roughness, *J. Geophys Res.*, *103*, 3217–3232, 1998.

Haller, M. C., R. A. Dalrymple, and I. A. Svendsen, Rip channels and nearshore circulation, in *Proceedings Coastal Dynamics'97*, pp. 594–603, Am. Soc. of Civ. Eng., New York, 1997.

Herbers, T. H. C., S. Elgar, and R. T. Guza, Directional spreading of waves in the nearshore, *J. Geophys. Res.*, *104*, 7683–7693, 1999.

Houwman, K. T., and P. Hoekstra, Tidal ellipses in the nearshore zone (-3 to -10 m); modelling and observations, in *Proceedings 26th International Coastal Engineering Conference*, pp. 773–786, Am. Soc. of Civ. Eng., New York, 1998.

Houwman, K. T., and L. C Van Rijn, Flow resistance in the coastal zone, *Coastal Eng* , *38*, 261–273, 1999.

Kuik, A. J., G. P. Van Vledder, and L. H. Holthuijsen, A method for the routine analysis of pitch-and-roll buoy wave data, *J. Phys. Oceanogr.*, *18*, 1020–1034, 1988.

Kuriyama, Y., and T. Nakatsukasa, A one-dimensional model for undertow and longshore current on a barred beach, *Coastal Eng.*, *40*, 39–58, 2000.

Lentz, S., R. T. Guza, S. Elgar, F. Feddersen, and T. H. C. Herbers, Momentum balances on the North Carolina inner shelf, *J. Geophys. Res.*, *104*, 18,205–18,226, 1999.

Lippmann, T. C., and R. A. Holman, The spatial and temporal variability of sandbar morphology, *J. Geophys. Res.*, *95*, 11,575–11,590, 1990.

Lippmann, T. C., E. B. Thornton, and A. J. R. M. Reniers, Wave stress and longshore current on barred profiles, in *Proceedings Coastal Dynamics'95*, pp. 401–412, Am. Soc. of Civ. Eng., New York, 1995.

Long, C. E., Index and bulk parameters for frequency-direction spectra measured at CERC Field Research Facility, June 1994 to August 1995, *Misc. Pap. CERC-96-6*, U.S. Army Eng. Waterw. Exp. Stn., Vicksburg, Miss., 1996.

Longuet-Higgins, M. S., Longshore currents generated by obliquely incident sea waves, *J. Geophys. Res.*, *75*, 6778–6789, 1970.

Longuet-Higgins, M. S., and R. W. Stewart, Radiation stress in water waves: A physical discussion with application, *Deep Sea Res.*, *11*, 529–563, 1964.

Nielsen, P., Analytical determination of nearshore wave height due to refraction, shoaling and friction, *Coastal Eng.*, *7*, 233–251, 1983.

Ozkan-Haller, H. T., and J. T. Kirby, Nonlinear evolution of shear instabilities of the longshore current: A comparison of observations and computations, *J. Geophys. Res.*, *104*, 25,953–25,984, 1999.

Reniers, A. J. H. M., and J. A. Battjes, A laboratory study of longshore currents over barred and non-barred beaches, *Coastal Eng.*, *30*, 1–22, 1997.

Sancho, F. E , I. A. Svendsen, A. R. Van Dongeren, and U. Petruvu, Longshore nonuniformities of nearshore currents, in *Proceedings Coastal Dynamics'95*, pp. 425–436, Am. Soc. of Civ. Eng., New York, 1995.

Sleath, J. F. A., *Sea Bed Mechanics*, John Wiley, New York, 1984.

Slinn, D. N., J. S. Allen, and R. A. Holman, Alongshore currents over variable beach topography, *J. Geophys. Res.*, *105*, 16,971–16,998, 2000.

Stive, M. J. F., and H. J. De Vriend, Shear stress and mean flow in shoaling and breaking waves, in *Proceedings 24th International Coastal Engineering Conference*, pp. 594–608, Am. Soc. of Civ. Eng., New York, 1994.

Svendsen, I. A., and U. Putrevu, Nearshore mixing and dispersion, *Proc. Roy. S. London, Ser. A*, *445*, 561–576, 1994.

Thornton, E. B., and R. T. Guza, Surf zone longshore currents and random waes: field data and models, *J. Phys. Oceanogr.*, *16*, 1165–1178, 1986.

Thornton, E. B., and C. S. Kim, Longshore currents and wave height modulation at tidal frequency inside the surfzone, *J. Geophys. Res.*, *98*, 16,509–16,519, 1993.

Walstra, D. J. R., G. P. Mocke, and F. Smit, Roller contributions as inferred from inverse modelling techniques, in *Proceedings 25th International Coastal Engineering Conference*, pp. 1205–1218, Am. Soc. of Civ. Eng., New York, 1996.

Whitford, D. J., and E. B. Thornton, Comparison of wind and wave forcing of longshore currents, *Cont. Shelf Res.*, *13*, 1205–1218, 1993.

S. Elgar, and F. Feddersen, Woods Hole Oceanographic Institution, Woods Hole, MA 02543, USA. (elgar@whoi.edu; falk@whoi.edu)

R. T. Guza, Center for Coastal Studies, Scripps Institution of Oceanography, University of California, La Jolla, CA 92093-0209, USA. (rtg@coast.ucsd.edu)

J. R. Miles, Institute of Marine Studies, University of Plymouth, Drake Circus, Plymouth PL4 8AA, United Kingdom. (j.r.miles@plymouth.ac.uk)

B. G. Ruessink, WL|Delft Hydraulics, Marine and Coastal Management, P. O. Box 177, 2600 MH Delft, Netherlands. (gerben.ruessink@wldelft.nl)

(Received December 12, 2000; revised June 14, 2001;
accepted June 14, 2001.)